D. N. BRASKI[1]

CONF-820628--5

DE82 017475

MICROSTRUCTURE AND TENSILE PROPERTIES OF NEUTRON-IRRADIATED $(Fe_{0.61}Ni_{0.39})_3V$ ORDERED ALLOY[2]

REFERENCE: Braski, D. N., "Microstructure and Tensile Properties of Neutron-Irradiated $(Fe_{0.61}Ni_{0.39})_3V$ Ordered Alloys," Effects of Radiation on Materials: Eleventh Conference ASTM STP 782, H. R. Brager and J. S. Perrin, Eds., American Society for Testing and Materials, 1982, pp. .

ABSTRACT: Small tensile specimens of the $(Fe_{0.61}Ni_{0.39})_3V$ long-range-ordered alloy were irradiated in the ORR to 4 dpa at 523, 623, and 823 K and subsequently tested at the same respective temperatures. The alloy remained ordered after irradiation at all three temperatures. Irradiation at 523 and 623 K increased the yield strength of the material by producing Frank loops in the microstructure and reduced the total elongation. The low strain hardening observed was attributed to planar slip and the absence of cross slip. Irradiation at 823 K embrittled the alloy. Premature failure was apparently initiated by helium bubbles on sigma phase boundaries which grew rapidly during the test to form microcracks. Fracture occurred after a microcrack propagated across grain boundaries that were weakened by helium and possibly sulfur. New LRO alloys without sigma phase should perform better under neutron irradiation.

KEY WORDS: long-range-ordered alloys, neutron irradiation damage, radiation hardening, helium embrittlement, sigma phase, Frank loops, planar slip, grain boundary segregation.

The long-range ordered $(Fe_{0.61}Ni_{0.39})_3V$ alloy (referred to hereafter as LRO16) has been developed at ORNL [1] for elevated temperature applications and is also a candidate for use in future fusion reactors. The alloy, which has an ordered $L1_2$ structure, demonstrates excellent tensile properties and extremely low creep rates below its critical ordering temperature (T_c) of ~943 K. The resistance of LRO16 to radiation damage was studied initially by bombarding disk specimens with 4 MeV nickel ions (70 dpa) while simultaneously injecting helium and deuterium [2]. Subsequent examination of the microstructure using transmission electron microscopy (TEM) showed that LRO16

ABSTRACT: Small tensile specimens of the $(Fe_{0.61}Ni_{0.39})_3V$ long-range-ordered alloy were irradiated in the ORR to 4 dpa at 523, 623, and 823 K and subsequently tested at the same respective temperatures. The alloy remained ordered after irradiation at all three temperatures. Irradiation at 523 and 623 K increased the yield strength of the material by producing Frank loops in the microstructure and reduced the total elongation. The low strain hardening observed was attributed to planar slip and the absence of cross slip. Irradiation at 823 K embrittled the alloy. Premature failure was apparently initiated by helium bubbles on sigma phase boundaries which grew rapidly during the test to form microcracks. Fracture occurred after a microcrack propagated across grain boundaries that were weakened by helium and possibly sulfur. New LRO alloys without sigma phase should perform better under neutron irradiation.

KEY WORDS: long-range-ordered alloys, neutron irradiation damage, radiation hardening, helium embrittlement, sigma phase, Frank loops, planar slip, grain boundary segregation.

The long-range ordered $(Fe_{0.61}Ni_{0.39})_3V$ alloy (referred to hereafter as LRO16) has been developed at ORNL [1] for elevated temperature applications and is also a candidate for use in future fusion reactors. The alloy, which has an ordered $L1_2$ structure, demonstrates excellent tensile properties and extremely low creep rates below its critical ordering temperature (T_c) of ~943 K. The resistance of LRO16 to radiation damage was studied initially by bombarding disk specimens with 4 MeV nickel ions (70 dpa) while simultaneously injecting helium and deuterium [2]. Subsequent examination of the microstructure using transmission electron microscopy (TEM) showed that LRO16 had less swelling below T_c than 20% cold-worked 316 stainless steel, but higher swelling above T_c [2]. This paper presents the results of an experiment aimed at measuring the resistance of LRO16 to neutron irradiation. Small tensile specimens of the alloy were irradiated for approximately one year in the ORR reactor at ORNL at temperatures of 523, 623, and 823 K and subsequently tested in tension at the same

[1]Metals and Ceramics Division, Oak Ridge National Laboratory, Oak Ridge, TN 37830.
[2]Research sponsored by the Office of Fusion Energy, U.S. Department of Energy, under contract No. W-7405-eng-26 with the Union Carbide Corporation.

temperatures in a radiation hot cell. TEM was used to observe the microstructural changes caused by the irradiation while scanning electron microscopy and Auger spectroscopy were employed to analyze the fracture surfaces.

EXPERIMENTAL

Specimen Fabrication

An ingot of the LRO16 alloy weighing ~0.4 kg was arc melted and cast under argon. The ingot was clad in molybdenum sheet, hot rolled at 1373 K, removed from the cladding, and cold rolled with intermediate anneals at 1373 K to a final sheet thickness of 0.76 mm. The sheet was annealed at 1403 K for 900 s and quenched in ice water to produce a disordered structure. The sheet was then aged at 878 K for 4.75×10^5 s (5.5 days) to produce the long-range-ordered (LRO) structure. Chemical analysis showed the composition by weight percent to be: 46 Fe, 31 Ni, and 23 V. The alloy also contained ~150 wt ppm of carbon which was present as an impurity. Small tensile specimens having 1.5 mm-wide gage sections (see ref. 3) were machined from the sheet.

Neutron Irradiation

The tensile specimens were exposed to a fluence of 4.8×10^{25} neutrons/m^2 (>0.1 MeV) in the ORR MFE-2 experiment conducted at this laboratory. The irradiation produced an atomic displacement level of ~4 dpa and ~29 at. ppm of helium in the material. The irradiation temperatures of 523, 623, and 823 K were measured and controlled by thermocouples and were within ± 5 K of the desired temperatures.

Postirradiation Tests and Analyses

An ingot of the LRO16 alloy weighing ~0.4 kg was arc melted and cast under argon. The ingot was clad in molybdenum sheet, hot rolled at 1373 K, removed from the cladding, and cold rolled with intermediate anneals at 1373 K to a final sheet thickness of 0.76 mm. The sheet was annealed at 1403 K for 900 s and quenched in ice water to produce a disordered structure. The sheet was then aged at 878 K for 4.75×10^5 s (5.5 days) to produce the long-range-ordered (LRO) structure. Chemical analysis showed the composition by weight percent to be: 46 Fe, 31 Ni, and 23 V. The alloy also contained ~150 wt ppm of carbon which was present as an impurity. Small tensile specimens having 1.5 mm-wide gage sections (see ref. 3) were machined from the sheet.

Neutron Irradiation

The tensile specimens were exposed to a fluence of 4.8×10^{25} neutrons/m^2 (>0.1 MeV) in the ORR MFE-2 experiment conducted at this laboratory. The irradiation produced an atomic displacement level of ~4 dpa and ~29 at. ppm of helium in the material. The irradiation temperatures of 523, 623, and 823 K were measured and controlled by thermocouples and were within ± 5 K of the desired temperatures.

Postirradiation Tests and Analyses

After the irradiation, the tensile specimens were tested under vacuum ($<10^{-5}$ Pa) in a hot cell Instron machine at the same respective temperatures used in the irradiation. The crosshead speed was 0.83 μm/s. Fracture surfaces were examined in a shielded SEM. Small disks were electrically discharged machined from both the shoulder and gage portions of the specimens for TEM examination. The disks were electropolished at 27 V dc in a 12.5 vol % solution of conc. H_2SO_4 in methanol at -30°C. The radioactivity levels of the disks were low enough to permit their examination in an unshielded TEM. One portion of a gage section which had been irradiated and tensile tested at 823 K was mounted in an Auger spectroscopy apparatus and broken again, in situ, at ~823 K to permit chemical analyses of the fracture surfaces. The Auger straining and analysis chambers were kept below 10^{-7} Pa during the entire experiment.

RESULTS

Postirradiation Tensile Properties

The results of the postirradiation tensile tests for LRO16 are listed in Table 1 and typical stress-strain curves for the unirradiated and irradiated material are given in Fig. 1. At 523 K, neutron irradiation increased the yield point significantly, or "hardened" the alloy (Fig. 1). The specimen subsequently deformed plastically with virtually no work hardening until failure occurred and the total elongation was less than half of that measured for the unirradiated specimen. The small amount of work hardening and somewhat early failures measured at 523 K produced ultimate tensile strengths that were all lower than the unirradiated material (Table 1). After irradiation at 623 K, LRO16 specimens were also hardened, but to a lesser degree than observed at the lower temperature. Their work-hardening behavior was closer to the unirradiated control specimen as demonstrated by the nearly parallel stress-strain curves. The ability of the irradiated specimens to undergo some strain hardening at 623 K enabled them to develop somewhat higher ultimate tensile strengths than found in the unirradiated alloy and values of elongation that were better than at 523 K (Table 1) Irradiation at 823 K produced no hardening and the stress-strain curves for the irradiated specimens followed that for the unirradiated material. However, failure occurred prematurely in all three specimens at relatively low values of strain. Consequently, the ultimate tensile strengths of these specimens were also reduced, as given in Table 1. The results in Table 1 are also shown graphically in Fig. 2. It is

Table 1. Results of Tensile Tests for Unirradiated and Irradiated LRO16

"hardened" the alloy (Fig. 1). The specimen subsequently deformed plastically with virtually no work hardening until failure occurred and the total elongation was less than half of that measured for the unirradiated specimen. The small amount of work hardening and somewhat early failures measured at 523 K produced ultimate tensile strengths that were all lower than the unirradiated material (Table 1). After irradiation at 623 K, LRO16 specimens were also hardened, but to a lesser degree than observed at the lower temperature. Their work-hardening behavior was closer to the unirradiated control specimen as demonstrated by the nearly parallel stress-strain curves. The ability of the irradiated specimens to undergo some strain hardening at 623 K enabled them to develop somewhat higher ultimate tensile strengths than found in the unirradiated alloy and values of elongation that were better than at 523 K (Table 1). Irradiation at 823 K produced no hardening and the stress-strain curves for the irradiated specimens followed that for the unirradiated material. However, failure occurred prematurely in all three specimens at relatively low values of strain. Consequently, the ultimate tensile strengths of these specimens were also reduced, as given in Table 1. The results in Table 1 are also shown graphically in Fig. 2. It is

Table 1. Results of Tensile Tests for Unirradiated and Irradiated LRO16

Specimen Number	Condition	Irradiation Test Temperature (K)	Yield Strength 0.2% Offset (MPa)	Ultimate Strength (MPa)	Uniform Elongation (%)	Total Elongation (%)
6-15	Unirradiated	523	367	988	26.1	26.2
6-16	Unirradiated	623	399	974	25.0	25.1
6-17	Unirradiated	823	419	899	30.8	31.3
6-2	Irradiated	523	875	882	7.9	9.9
6-3	Irradiated	523	866	878	9.3	11.6
6-5	Irradiated	523	879	894	9.2	10.0
6-6	Irradiated	623	650	1074	13.0	13.6
6-7	Irradiated	623	684	1083	12.9	13.5
6-8	Irradiated	623	834	1123	11.2	11.8
6-9	Irradiated	823	441	475	2.6	2.9
6-11	Irradiated	823	431	526	4.1	4.4
6-14	Irradiated	823	441	465	0.9	1.1

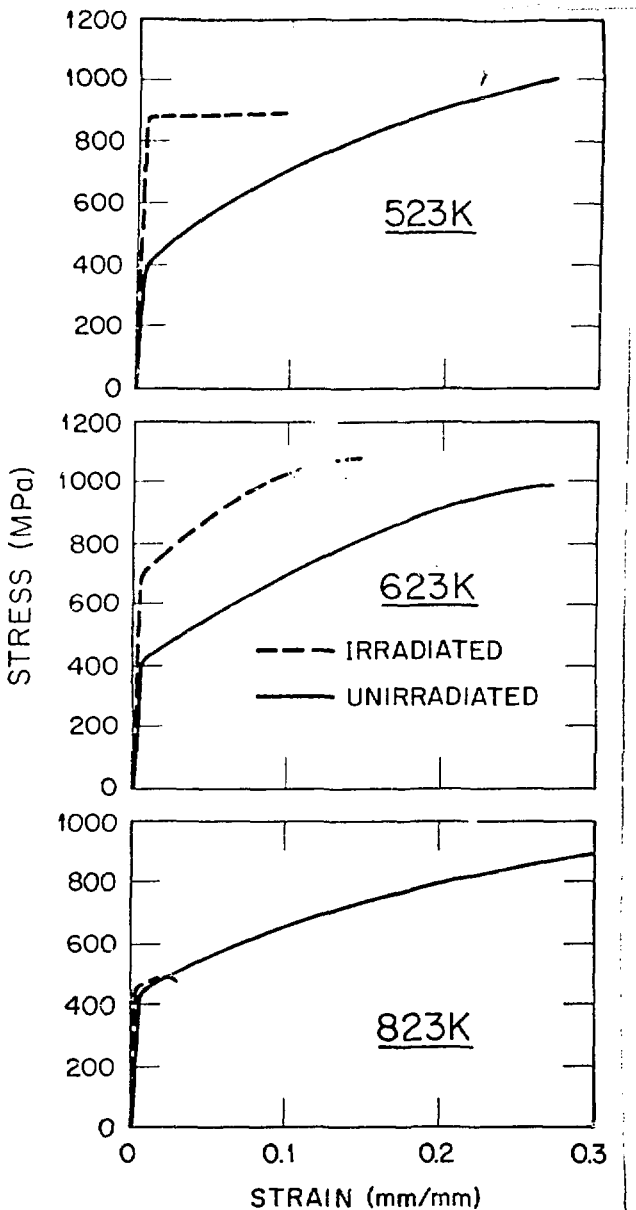

Fig. 1-Stress-strain curves for unirradiated LRO16 and for LRO16 which was irradiated to 4 dpa in ORR at 523, 623, and 823 K and tested at the same respective temperatures.

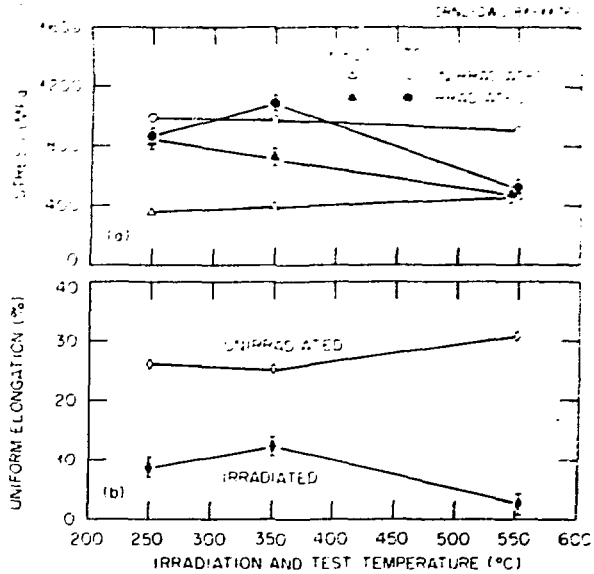

Fig. 2-Tensile properties of unirradiated and irradiated LRO 16 as a function of temperature. The irradiated specimens were tensile tested at the same temperature that they were irradiated.

interesting to note that the yield strength of the unirradiated LRO16 increased with temperature. This somewhat unusual feature is characteristic of LRO alloys and will be discussed in conjunction with the microstructure later. Summarizing the effects of the neutron irradiation: irradiation at 523 and 623 K hardened the LRO16 alloy causing moderate losses in ductility, while irradiation at 823 K produced no hardening but even greater losses of ductility. The next section of this paper presents the results of various microstructural analyses that were conducted to help understand the effects of neutron irradiation on the mechanical properties.

Microstructural Analyses

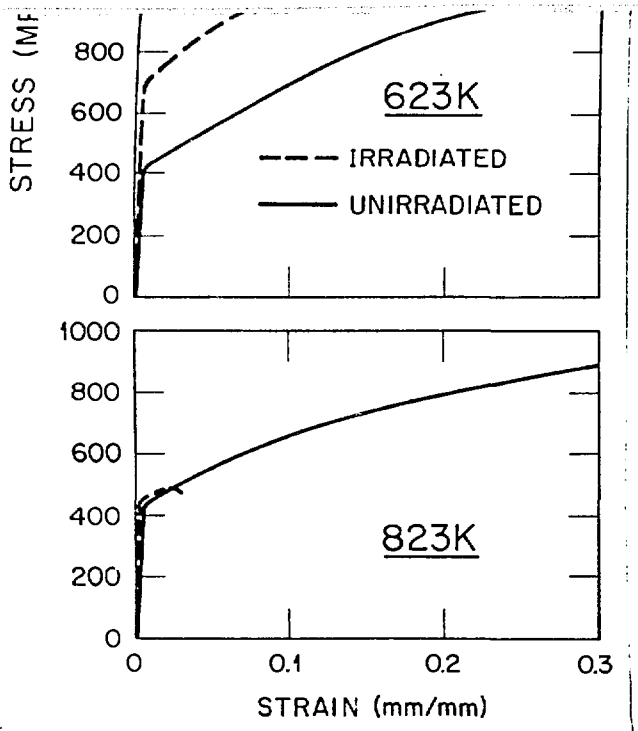

Fig. 1-Stress-strain curves for unirradiated LRO16 and for LRO16 which was irradiated to 4 dpa in ORR at 523, 623, and 823 K and tested at the same respective temperatures.

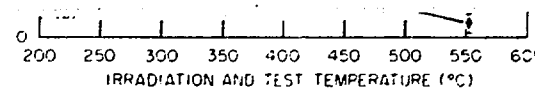

Fig. 2-Tensile properties of unirradiated and irradiated LRO 16 as a function of temperature. The irradiated specimens were tensile tested at the same temperature that they were irradiated.

interesting to note that the yield strength of the unirradiated LRO16 increased with temperature. This somewhat unusual feature is characteristic of LRO alloys and will be discussed in conjunction with the microstructure later. Summarizing the effects of the neutron irradiation: irradiation at 523 and 623 K hardened the LRO16 alloy causing moderate losses in ductility, while irradiation at 823 K produced no hardening but even greater losses of ductility. The next section of this paper presents the results of various microstructural analyses that were conducted to help understand the effects of neutron irradiation on the mechanical properties.

Microstructural Analyses

Transmission Electron Microscopy

The unirradiated microstructure of LRO16 is shown in Fig. 3. It is composed of an ordered matrix containing small particles of vanadium carbide (diam ≅ 25nm) and grain boundaries lined with similar particles (Fig. 3a). The identification of the particles as VC was supported by both electron diffraction and energy dispersive x-ray analyses [2]. The carbide particles had a cube-on-cube orientation relationship with the matrix

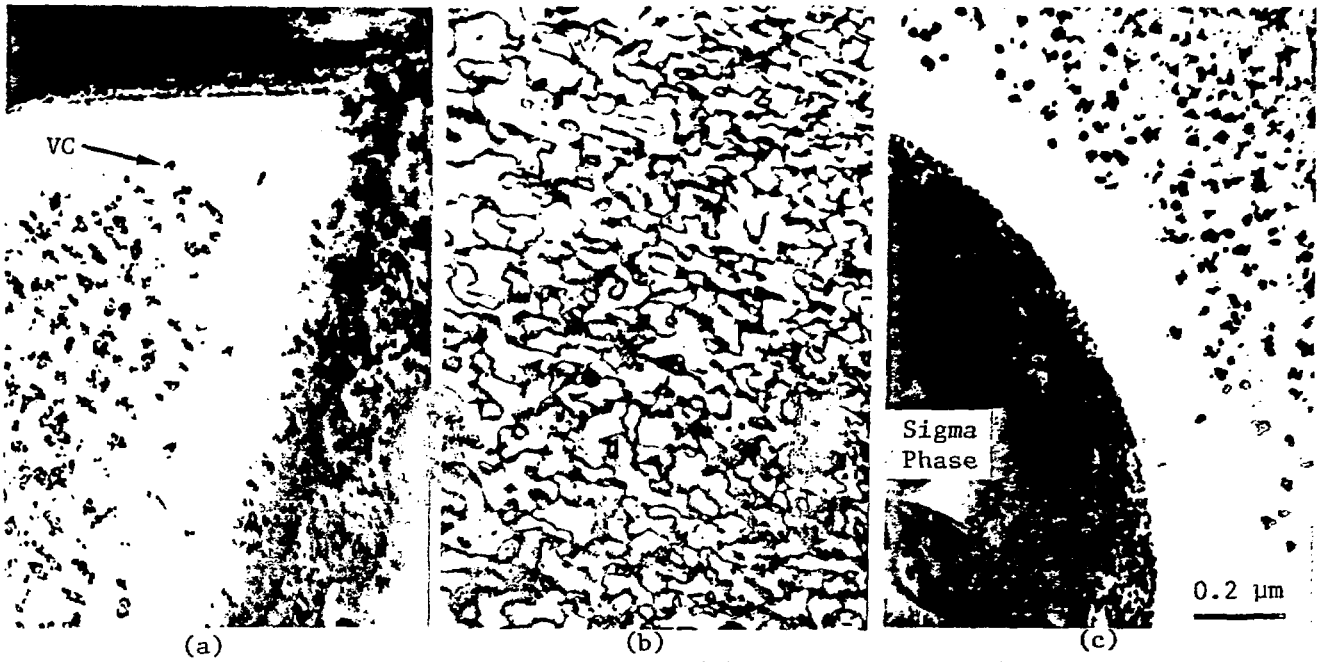

Fig. 3-Microstructure of unirradiated LR016. (a) Bright field, (b) dark field using superlattice (100) reflection, and (c) bright field showing sigma phase.

and produced strain contrast in the electropolished foil. Narrow zones on both sides of grain boundaries were denuded of VC particles (Fig. 3a). Figure 3b shows the ordered matrix of the alloy imaged using a (100) superlattice reflection in the dark field mode. The ordered domains and two-thirds of the antiphase boundaries (APBs) can be seen. When all of the APBs are imaged simultaneously, the ordered domains are equiaxed in shape. The average domain size was ~42 nm in diameter and the APBs had a/2<110> displacement vectors [4]. The microstructure also contained scattered regions of sigma phase as shown in Fig. 3c. Selected area diffractions showed that the sigma phase was tetragonal with a_o = 0.88nm and co = 0.46 nm [2]. Energy dispersive X-ray analyses showed that the composition of the sigma was primarily Fe and V with some Ni [2]. It was observed that the sigma phase regions were often faulted.

The effects of neutron irradiation on the microstructure at the three different temperatures are shown in Fig. 4. Quantitative measurements obtained from these and other micrographs are listed in Table II. Irradiation at 523 K produced a relatively high density (4.1×10^{22} m^{-3}) of small dislocation loops (diam ≅ 12.0 nm) in an ordered matrix as shown in Fig. 4a. A few larger loops displayed fringes indicating they were faulted. Within the resolution of the electron microscope (~1 nm), no cavities were observed. Irradiation at 523 K as well as the two higher temperatures, caused most of the VC within the grains to dissolve. Such a phenomenon was probably due to the cascade processes driving precipitate atoms back into solution [5]. On the other hand,

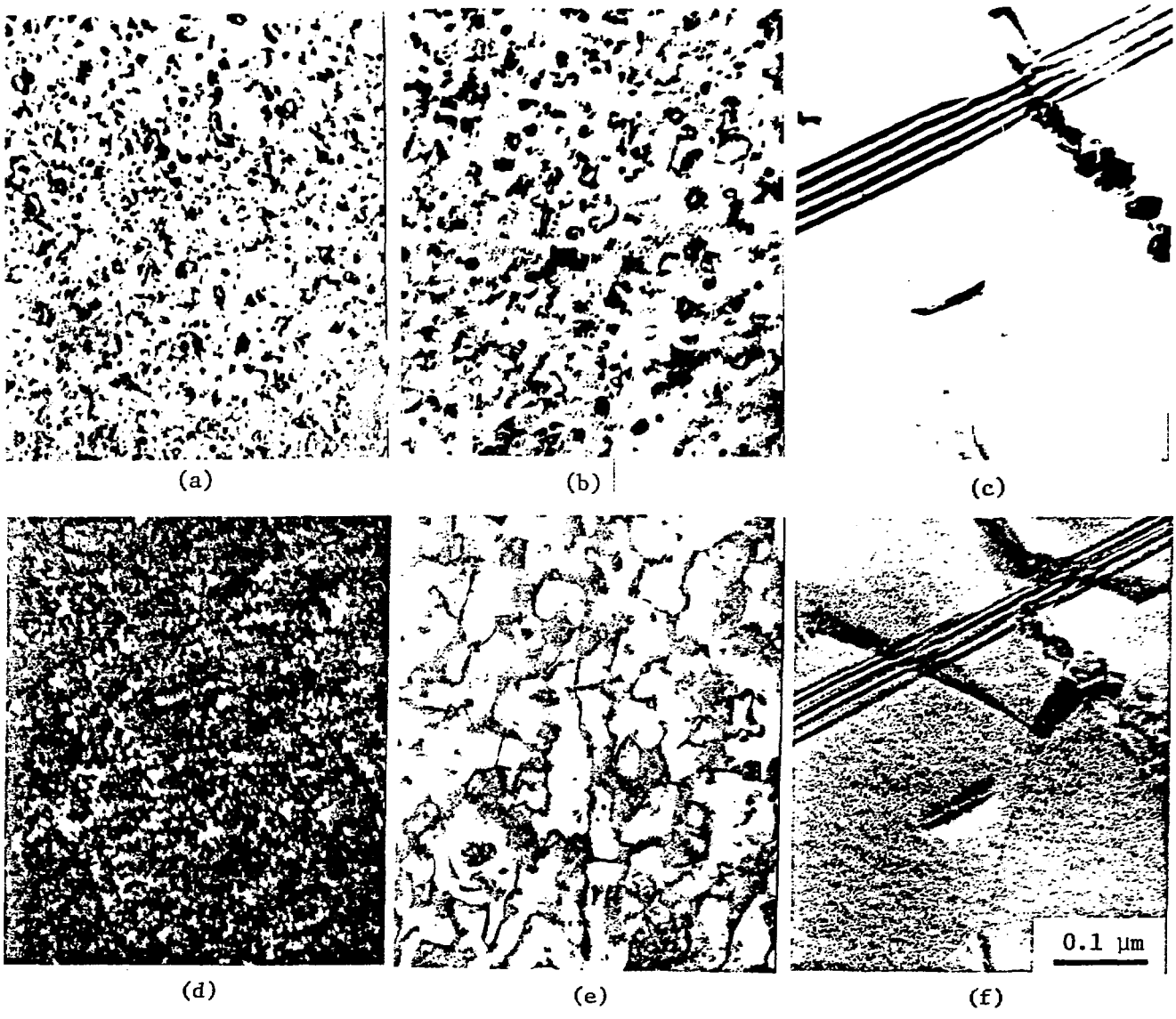

Fig. 4-Microstructure of irradiated LR016 shown in bright field for irradiation temperatures of (a) 523 K, (b) 623 K, and (c) 823 K. Ordered domains shown in superlattic dark field for the same specimens at (d) 523 K, (e) 623 K, and (f) 823 K.

Table 2. Quantitative Microstructural Data for Irradiated LR016

Irradiation Test Temperature (K)	Loop Density (m^{-3})	Average Loop Diameter (nm)	Average Domain Size (nm)	Average Cavity Diameter (nm)	Swelling (%)
523	4.1×10^{22}	12.0	7.5	--	0
623	1.3×10^{22}	26.4	25.2	3.3	0.01
823	9.2×10^{19}	233.6	238.9	5.9	0.07

the VC particles in the grain boundaries were coarsened. At 623 K, (Fig. 4b), less than half the number of loops were produced, but their average size of 26.4 nm was larger than at 523 K. The loops were faulted and interstitial in nature. A few cavities having average diameters of 3.3 nm were observed, resulting in approximately 0.01% swelling. Again, the structure retained its long-range-ordered structure.

At 823 K smaller numbers of larger-sized faulted loops were produced, as shown in Fig. 4c and Table II. Although most of the faulted loops were interstitial, approximately 10% were vacancy type. Not enough loops were analyzed at the lower temperature to establish whether some were vacancy type. A few cavities were observed that produced 0.07% swelling. Figures 4d, 4e and 4f show the ordered domains in LRO16 after irradiation at 523, 623, and 823 K, respectively. The domains were effectively subdivided from their original size by the irradiation at the lowest temperature, and they increased in size with increasing temperature. This has been observed previously in an ion-irradiated cobalt-base LRO alloy [7] and is attributed to subdivision of the original domains by radiation-induced stacking faults which also serve as APBs. At 823 K the larger size of the domains was due to thermal growth [4], tempered by the few stacking faults. An interstitial faulted loop/APB has a different displacement vector (i.e. a/3 <111>) compared to a thermal APB (a/2<110>) and somewhat lower energy [4]. Therefore, the average domain size was controlled mainly by number and size of loops which, in turn, was a function of temperature. The average domain size turned out to be nearly the same as the average loop size and both increased with increasing irradiation temperature (see Table II).

Some effects of plastic deformation at 823 K on the irradiated microstructure of LRO16 are illustrated in Figs. 5 and 6. Figure 5 shows the effect of plastic deformation on typical grain boundaries. After irradiation (Fig. 5a), the grain boundaries

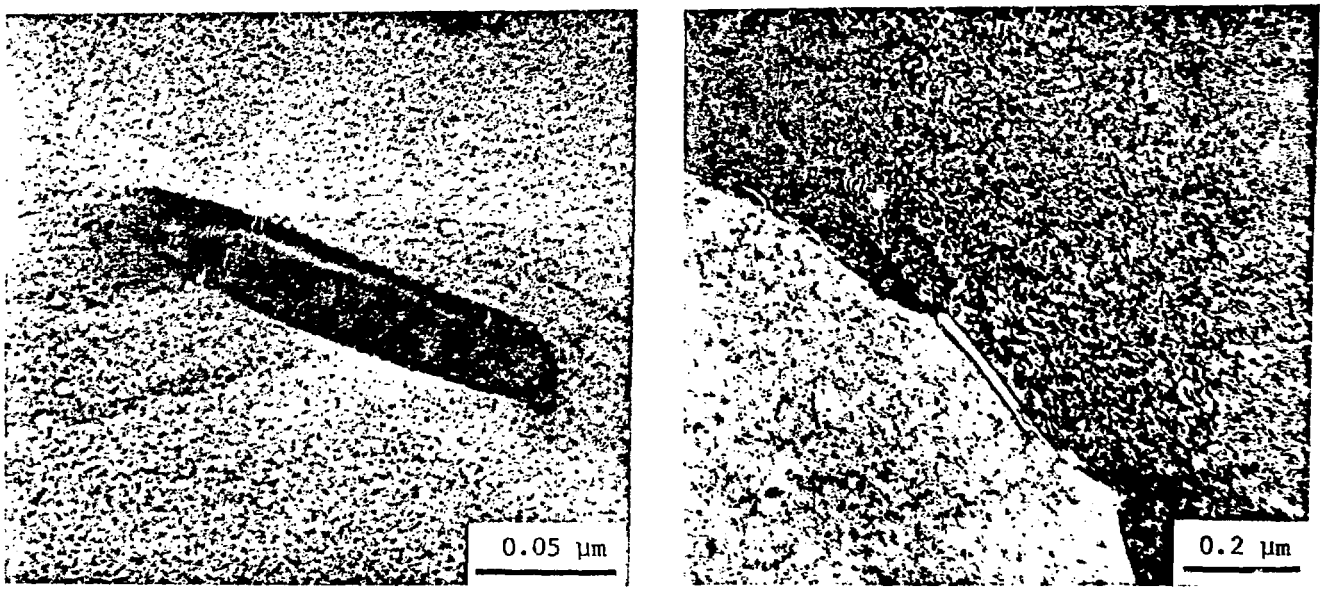

(a) (b)

Fig. 5-(a) Grain boundary in LRO16 containing a VC particle and small helium bubbles after irradiation at 823 K. Note the bubbles attached to the periphery of the VC particle. (b) Grain boundary in LRO16 after irradiation and testing at 823 K showing how the particles were etched out during specimen preparation.

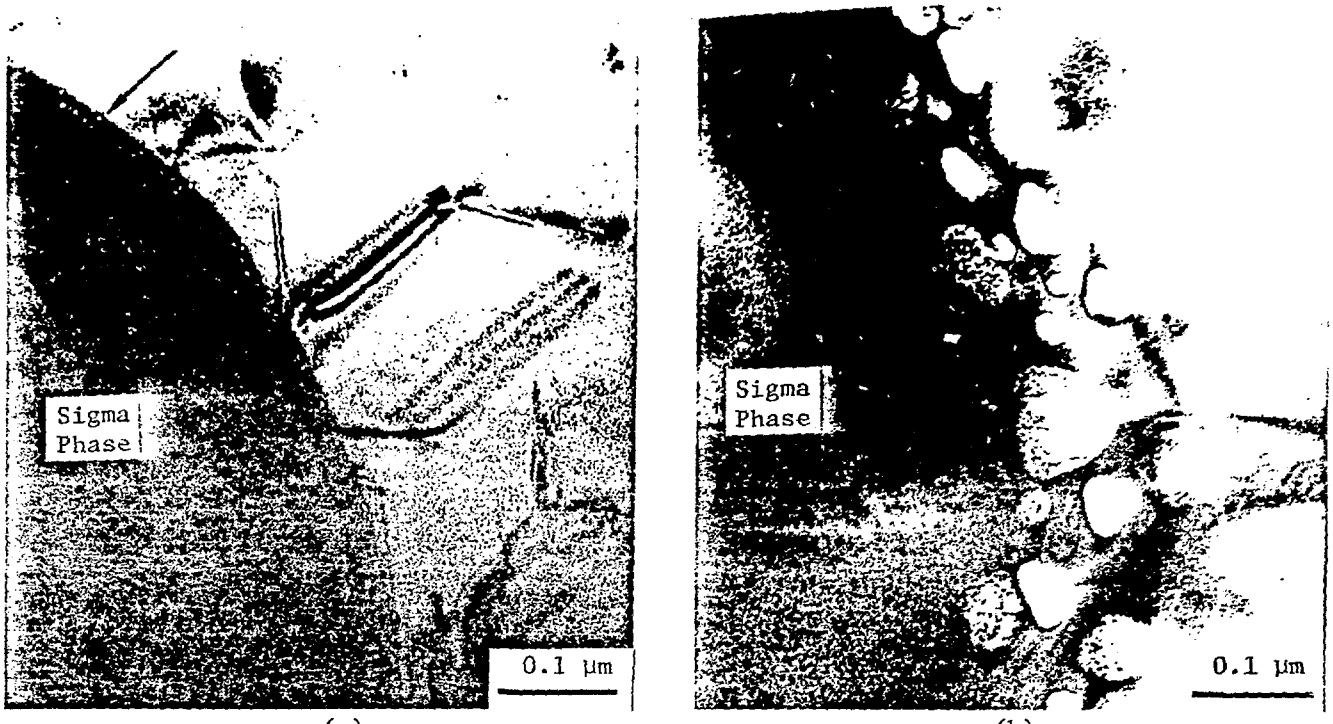

Fig. 6-Sigma phase/matrix boundary in LR016 (a) containing small helium bubbles after irradiation at 823 K, and (b) after postirradiation tensile testing at 823 K showing how the bubbles have grown.

contained numerous cavities (probably helium bubbles) and thin lath-shaped VC particles. Small helium bubbles were often attached to the periphery of the VC laths as shown in the figure. Plastic deformation caused the VC laths to be preferentially etched out during specimen preparation as shown in Fig. 5b. Perhaps the bubbles attached to the laths grew during testing and coalesced. This would make the VC interfaces more susceptible to the electrochemical attack. Another possibility is that the bubble-weakened interfaces enabled the harder VC laths to separate physically from the softer metal matrix, thus enabling the laths to be easily etched out. It should be pointed out that the cavities or bubbles in the grain boundaries were not actually observed to undergo any significant growth after the elevated temperature deformation. This was not the case with sigma phase boundaries as illustrated in Fig. 6. After irradiation, the interfaces separating sigma phase from the matrix also contained numerous small cavities or bubbles (Fig. 6a). However, the tensile test at 823 K caused the cavities to grow an order of magnitude in size as shown in Fig. 6b. All of the sigma phase region in the foil had either large cavities attached or were etched preferentially (due to the cavities).

Fig. 6-Sigma phase/matrix boundary in LR016 (a) containing small helium bubbles after irradiation at 823 K, and (b) after postirradiation tensile testing at 823 K showing how the bubbles have grown.

contained numerous cavities (probably helium bubbles) and thin lath-shaped VC particles. Small helium bubbles were often attached to the periphery of the VC laths as shown in the figure. Plastic deformation caused the VC laths to be preferentially etched out during specimen preparation as shown in Fig. 5b. Perhaps the bubbles attached to the laths grew during testing and coalesced. This would make the VC interfaces more susceptible to the electrochemical attack. Another possibility is that the bubble-weakened interfaces enabled the harder VC laths to separate physically from the softer metal matrix, thus enabling the laths to be easily etched out. It should be pointed out that the cavities or bubbles in the grain boundaries were not actually observed to undergo any significant growth after the elevated temperature deformation. This was not the case with sigma phase boundaries as illustrated in Fig. 6. After irradiation, the interfaces separating sigma phase from the matrix also contained numerous small cavities or bubbles (Fig. 6a). However, the tensile test at 823 K caused the cavities to grow an order of magnitude in size as shown in Fig. 6b. All of the sigma phase region in the foil had either large cavities attached or were etched preferentially (due to the cavities).

Scanning Electron Microscopy

Scanning electron micrographs of fracture surfaces from LR016 specimens tensile-tested after irradiation are shown in Fig. 7. Figures 7a, b, and c show the fractures of unirradiated specimens tested at 523, 623 and 823 K, respectively. Figures 7d, e,

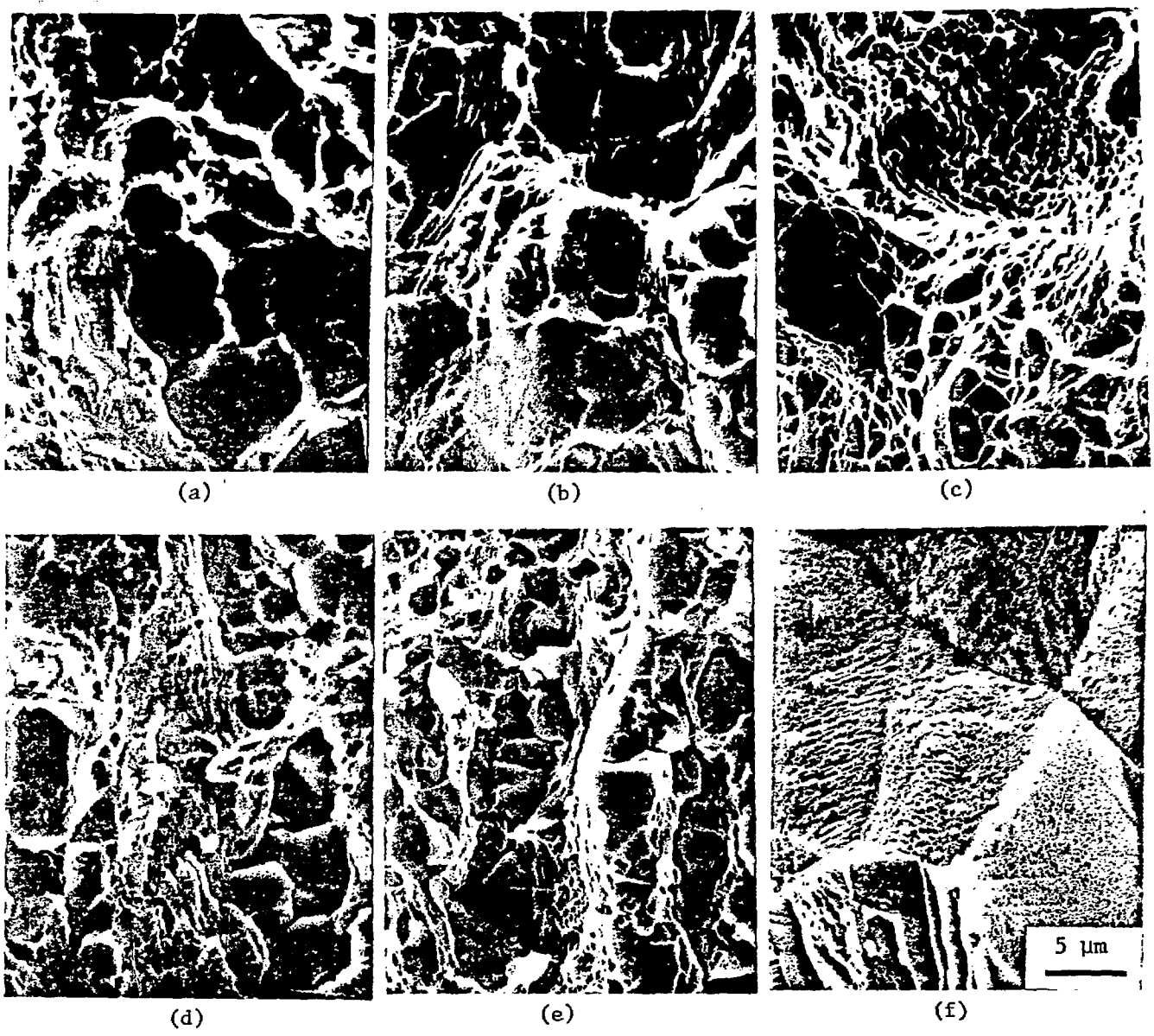

Fig. 7-Fracture surfaces of unirradiated LRO16 specimens that were tensile tested at (a) 523 K, (b) 623 K, and (c) 823 K, and fracture surfaces of LRO16 specimens that were irradiated and tensile tested at (d) 523 K, (e) 623 K, and (f) 823 K.

and f show the fractures of specimens which were irradiated before testing at the same temperatures. Unirradiated LRO16 that was tested at 523 and 623 K (Figs. 7a and 7b) had similar fracture surfaces — i.e., ductile "dimples" mixed with some small flat facets. These facets are believed to be caused by fracture along or across the stronger, but more brittle sigma phase. At 823 K (Fig. 7c), the fracture surfaces were entirely dimpled which is characteristic of ductile fracture. Irradiation produced no significant changes in the appearances of fracture surfaces at 523 and 623 K (Figs. 7d

The gage section from an LRO16 specimen that had been irradiated and tested at 823 K was mounted in an Auger spectroscopy system and pulled in tension at 823 K until failure resulted. The resulting fracture surfaces contained intergranular areas similar to Fig. 7f as well as mixed ductile-intergranular areas. The Auger analyses from each of these areas are given in Table 3. One of the Auger peaks was located at a position that corresponds to both boron and chlorine and we were unable to determine which element was actually present. For computational purposes, the table was calculated with the assumption that the questionable element was boron. Initially (time = 0), the intergranular areas show twice as much sulfur as the mixed areas and both areas show moderately high concentrations of boron. After sputtering material off the fracture surfaces for 120 s, the boron concentration dropped significantly while that of sulfur remained unchanged. After an additional 240 s of sputtering, the amounts of sulfur were markedly reduced, while the boron concentrations experienced smaller decreases. While sputtering reduced sulfur and boron, the concentrations of carbon and vanadium increased for both areas. A possible interpretation of these results is given as follows: Sulfur was segregated to grain boundaries and therefore showed a higher concentration in the predominantly intergranular area. As the surface layers were eroded away by sputtering, the sulfur peak decreased as new material within the grains was exposed. At the same time, the sputtering exposed a greater portion of the existing VC particles along the grain boundaries and the vanadium and carbon peaks increased. However, with the uncertainties associated with the rapid diffusion of sulfur in the elevated temperature test, one cannot be sure that sulfur was actually segregated at the grain boundaries. Moreover, since only an irradiated specimen was analyzed, it was not possible to determine if segregation was caused by the irradiation or by thermal aging. Clearly, more work needs to be done in the area of Auger analysis before a more definite conclusion can be made concerning sulfur segregation. With

Table 3. Auger Spectroscopy Results

Area	Sputtering Time (s)	S	B (or Cl)	C	V	Fe	Ni
Intergranular	0	0.6	26.8	16.3	13.4	23.1	19.8
	120	0.6	14.8	21.1	17.0	26.6	19.9
	360	0.2	12.1	20.6	18.9	27.7	20.5
Mixed-ductile Intergranular	0	0.3	29.2	16.7	12.7	23.3	17.8
	120	0.3	12.9	21.4	17.5	28.4	19.6
	360	0.1	6.5	22.6	19.7	30.5	20.6

regard to helium, a small amount was detected by the residual gas analyses when the specimen fractured. It is not unreasonable to assume that the numerous cavities observed by TEM on sigma phase and grain boundaries were helium bubbles, and that a small amount of this helium gas was released at fracture.

DISCUSSION

From an engineering standpoint the unirradiated LRO16 alloy demonstrated good mechanical properties in the 523–973 K temperature range. A rather unique property of LRO16 and other LRO alloys is that their yield strength increases, rather than decreases, with temperature (Fig. 2). The mechanism causing this phenomenon is believed to be related to the decrease in degree of order as the temperature is increased towards the critical order-disorder temperature, T_c [7]. As the degree of order is decreased, the spacing between pairs of dislocations making up the superdislocations becomes larger and the dislocation must do more work against the ordering forces since they will leave behind more APB [7,8].

At 523 K, neutron irradiation hardened the grain matrices by producing relatively large numbers of small interstitial (Frank) loops (Fig. 4a). Fewer loops and somewhat less hardening occurred at 623 K (Fig. 4b). It is well known that a high density of small defects in the microstructure serves as obstacles to dislocation movement and that their introduction will increase the yield stress or "harden" a material. The small loops were also APB and their presence effectively reduced the unirradiated domain size of 42 nm to 7.5 and 25.2 nm after irradiation at 523 and 623 K, respectively. The movement of a superdislocation through an ordered domain increases the domain boundary area and the stress required to accomplish this is a function of domain size [9]. A maximum hardness in Cu_3Au was observed by Biggs and Broom [10] for 5-nm-diam domains, and by Davies and Stoloff [11] for 3.5-nm-diam domains. Since the ordered domains in LRO16 were reduced in size during irradiation to 7.5 nm, it would appear that a portion of the overall hardening could be also attributed to domain

DISCUSSION

From an engineering standpoint the unirradiated LRO16 alloy demonstrated good mechanical properties in the 523–623 K temperature range. A rather unique property of LRO16 and other LRO alloys is that their yield strength increases, rather than decreases, with temperature (Fig. 2). The mechanism causing this phenomenon is believed to be related to the decrease in degree of order as the temperature is increased towards the critical order-disorder temperature, T_c [7]. As the degree of order is decreased, the spacing between pairs of dislocations making up the superdislocations becomes larger and the dislocation must do more work against the ordering forces since they will leave behind more APB [7,8].

At 523 K, neutron irradiation hardened the grain matrices by producing relatively large numbers of small interstitial (Frank) loops (Fig. 4a). Fewer loops and somewhat less hardening occurred at 623 K (Fig. 4b). It is well known that a high density of small defects in the microstructure serves as obstacles to dislocation movement and that their introduction will increase the yield stress or "harden" a material. The small loops were also APB and their presence effectively reduced the unirradiated domain size of 42 nm to 7.5 and 25.2 nm after irradiation at 523 and 623 K, respectively. The movement of a superdislocation through an ordered domain increases the domain boundary area and the stress required to accomplish this is a function of domain size [9]. A maximum hardness in Cu_3Au was observed by Biggs and Broom [10] for 5-nm-diam domains, and by Davies and Stoloff [11] for 3.5-nm-diam domains. Since the ordered domains in LRO16 were reduced in size during irradiation to 7.5 nm, it would appear that a portion of the overall hardening could be also attributed to domain hardening. Although this seems to be a reasonable conclusion, its validity depends on the way in which loop/APBs interact with superdislocations. The loop/APBs are structural defects as well as lines of discontinuity in the ordered lattice, so their interaction with superdislocations would be expected to be somewhat different. Since the APB energy of a loop/APB is less than a thermal APB [4] (i.e., the disordering atom displacements for loop/APBs are further away than nearest neighbor ones) one would spe-

any case, domain hardening probably contributed, in some measure, to the total irradiation hardening. The degree of hardening after irradiation showed up clearly in the mechanical tests by the upward shift of the stress-strain curves as shown in Fig. 1 for 523 and 623 K. Because the material was substantially hardened by irradiation at 523 K, it reached quite high stress levels before yielding. Then the material deformed plastically with virtually no strain hardening so that the ultimate strength was nearly identical to the yield strength. This interesting deformation behavior may be due to a process involving primarily planar slip. Fine deformation bands all running in the same direction within a single grain, were observed by TEM in the tested gage section of the irradiated specimen. Some of the bands were selectively etched out during foil preparation as shown in Fig. 8. It is not clear whether these etched-out areas were removed because of high localized strains or if there were actually deformation-induced voids in these areas. In any event, the planar nature of the deformation is evident with no signs of cross slip. The possibility of strain-induced disorder was also considered as a possible explanation for the lack of strain hardening at 523 K. In that situation, strain-induced disorder would permit cross slip of ordinary dislocations and cause little work hardening, where cross slip would be discouraged in the ordered lattice, with superlattice dislocations [12]. However, this mechanism does not appear to apply to the LRO16 results at 523 K because: (1) both irradiated and unirradiated specimens remained ordered after tensile tesing, (2) the stress-strain curve for the unirradiated specimen would have also leveled off at some intermediate value of strain due to disordering, and this did not happen, and (3) there was no evidence of cross slip in the deformed

process involving primarily planar slip. Fine deformation bands all running in the same direction within a single grain, were observed by TEM in the tested gage section of the irradiated specimen. Some of the bands were selectively etched out during foil preparation as shown in Fig. 8. It is not clear whether these etched-out areas were removed because of high localized strains or if there were actually deformation-induced voids in these areas. In any event, the planar nature of the deformation is evident with no signs of cross slip. The possibility of strain-induced disorder was also considered as a possible explanation for the lack of strain hardening at 523 K. In that situation, strain-induced disorder would permit cross slip of ordinary dislocations and cause little work hardening, where cross slip would be discouraged in the ordered lattice, with superlattice dislocations [12]. However, this mechanism does not appear to apply to the LRO16 results at 523 K because: (1) both irradiated and unirradiated specimens remained ordered after tensile tesing, (2) the stress-strain curve for the unirradiated specimen would have also leveled off at some intermediate value of strain due to disordering, and this did not happen, and (3) there was no evidence of cross slip in the deformed microstructure. At 623 K, the shape of the stress-strain curves for irradiated and unirradiated specimens was the same except that the curve for the irradiated one was shifted to higher stress levels due to irradiation hardening.

Fig. 8. Selectively etched deformation bands in LRO16 specimen that was irradiated and tensile tested at 523 K. Foil sample was prepared from gage section of tensile specimen after testing.

At this temperature, the hardening was not as great as observed at 523 K because of the smaller number of loops present and a larger domain size.

Fracture occurred in LRO16 at the two lower temperatures by ductile tearing and the coalescence of microvoids as shown by SEM (Fig. 7). Some cracking along sigma phase/matrix interfaces or through the sigma phase itself probably occurred as well, and is thought to account for the flat facets seen in the fractographs for both unirradiated and irradiated material. There was no evidence, from either SEM or TEM, that helium played a major role in the fracture at 523 or 623 K. However, helium in the form of very tiny bubbles (unresolvable at 523 K) may have influenced fracture indirectly by adding to the matrix hardening.

After irradiation at 823 K, the microstructure contained a relatively small number of larger loops (Table 2 and Fig. 4c). The structure was well ordered (strong superlattice reflection) and the ordered domain size had grown substantially (cf. Fig. 4d with 3b). Earlier work [4] on a cobalt-base LRO alloy showed that such growth was due to thermal aging. The amount of swelling was only 0.07%. Since the irradiated microstructure presented very few obstacles to dislocation motion, the stress-strain curves for this temperature were essentially identical to the unirradiated material (Fig. 1). However, the specimens failed prematurely after relatively low strains. The early failures were probably caused by the early formation of microcracks at sigma phase boundaries. This hypothesis is based on the observation of the very large cavities located at the sigma-phase/matrix boundaries after testing at 823 K (Fig. 6b). The cavities grew from the small cavities or helium bubbles produced by irradiation. The cavities grew by accumulating vacancies and perhaps more helium during the deformation process and they eventually coalesced to form microcracks. Helium bubbles located in the grains and grain boundaries did not appear to grow as did those on sigma phase boundaries. The helium bubbles attached to grain boundary VC particles did, however, influence preparation of the foils and nearly all of the VC particles were etched out of the foil (Fig. 5b). Growth of cavities on sigma phase boundaries, but

After irradiation at 823 K, the microstructure contained a relatively small number of larger loops (Table 2 and Fig. 4c). The structure was well ordered (strong superlattice reflection) and the ordered domain size had grown substantially (cf. Fig. 4d with 3b). Earlier work [4] on a cobalt-base LRO alloy showed that such growth was due to thermal aging. The amount of swelling was only 0.07%. Since the irradiated microstructure presented very few obstacles to dislocation motion, the stress-strain curves for this temperature were essentially identical to the unirradiated material (Fig. 1). However, the specimens failed prematurely after relatively low strains. The early failures were probably caused by the early formation of microcracks at sigma phase boundaries. This hypothesis is based on the observation of the very large cavities located at the sigma-phase/matrix boundaries after testing at 823 K (Fig. 6b). The cavities grew from the small cavities or helium bubbles produced by irradiation. The cavities grew by accumulating vacancies and perhaps more helium during the deformation process and they eventually coalesced to form microcracks. Helium bubbles located in the grains and grain boundaries did not appear to grow as did those on sigma phase boundaries. The helium bubbles attached to grain boundary VC particles did, however, influence preparation of the foils and nearly all of the VC particles were etched out of the foil (Fig. 5b). Growth of cavities on sigma phase boundaries, but not elsewhere in the microstructure, may be related to the deformation process. Deformation of the matrix around the brittle sigma phase areas may have readily occurred, but little grain boundary sliding may have taken place because of the many VC particles present to obstruct sliding. Studies of bubble growth [13] have indicated that rapid helium bubble growth will occur where sliding is taking place. Nevertheless, the lack of cavity growth in grain boundaries does not mean that the

structural integrity of the boundaries was preserved. In fact, the opposite was probably true as the helium acted to reduce cohesion forces between adjacent grains or perhaps inhibited "healing" of microcracks which eventually open up in grain boundaries, as suggested by Kangilaski et al. [14] Weakening of the grain boundaries was evidenced by the intergranular fracture observed by SEM (Fig. 7f). Another mechanism may have been acting in concert with helium to weaken the grain boundaries during irradiation at 823 K — that is, the segregation of sulfur to grain boundaries. The preliminary Auger analyses show the presence of sulfur on fractures surfaces that was subsequently reduced by sputtering. The embrittling effects of sulfur in nickel-base alloys are well known and its possible involvement in the irradiation embrittlement of LRO16 should not be overlooked.

The hardening of the LRO16 alloy by neutron irradiation at 523 and 623 K and embrittlement at 823 K parallels the behavior of other structural materials such as austenitic stainless steel [15]. Even though the embrittlement of LRO16 at elevated temperatures may not be eliminated entirely, more advanced LRO alloys are expected to demonstrate better resistance to this problem. These newer alloys have higher nickel contents and they may be prepared in such a way as to eliminate the presence of sigma-phase [2]. Without sigma-phase in the microstructure, the nucleation of microcracks will hopefully be delayed and more deformation can be accommodated before failure occurs. In addition, LRO alloys free of sigma-phase, appear to have better resistance to swelling [2].

The hardening of the LRO16 alloy by neutron irradiation at 523 and 623 K and embrittlement at 823 K parallels the behavior of other structural materials such as austenitic stainless steel [15]. Even though the embrittlement of LRO16 at elevated temperatures may not be eliminated entirely, more advanced LRO alloys are expected to demonstrate better resistance to this problem. These newer alloys have higher nickel contents and they may be prepared in such a way as to eliminate the presence of sigma-phase [2]. Without sigma-phase in the microstructure, the nucleation of microcracks will hopefully be delayed and more deformation can be accommodated before failure occurs. In addition, LRO alloys free of sigma-phase, appear to have better resistance to swelling [2].

SUMMARY

The LRO16 specimens remained ordered after neutron irradiation at 523 and 623 K but were hardened because of the relatively large numbers of interstitial faulted (Frank) loops produced in the microstructure. These loops were also APBs in the ordered structure, so a decrease or refinement in ordered domain size resulted. This reduction in domain size may have also contributed to the hardening. The hardening affected subsequent tensile tests at 523 and 623 K by shifting the stress-strain curves upward. At 523 K, deformation of the irradiated LRO16 produced virtually no strain hardening and appeared to involve planar slip with little or no cross slip.

Irradiation at 823 K produced no observable changes in long-range order, a rather large domain size, and a few relatively large loops that were mostly interstitial. The stress-strain curves for these specimens were identical to those for the unirradiated control specimen except that failure occurred after very low strains. The premature

failure appeared to be initiated by the presence of cavities at sigma phase boundaries which grew rapidly during the tensile test to form microcracks. A given microcrack then propagated through grain boundaries that were weakened by the presence of helium and possibly sulfur. New LRO alloys without sigma phase are expected to perform better under elevated temperature neutron irradiation.

ACKNOWLEDGMENTS

The author is indebted to C. T. Liu for supplying the material, B. L. Cox and L T. Gibson for specimen preparation and testing, L. Shrader for the SEM micrographs, L. Heatherly and R. E. Clausing for the Auger analysis, and K. Farrell and E. E. Bloom for helpful discussions.

REFERENCES

[1] Liu, C. T., J. Nucl. Mater. 85&86 (1979) 907–911.

[2] Braski, D. N., The Resistance of $(Fe,Ni)_3V$ Long-Range Ordered Alloys to Neutron and Ion Irradiation, Proc. 2nd Topical Meeting - Fusion Reactor Materials, Seattle, Washington, 1981, to be published in Journal of Nuclear Materials.

[3] Grossbeck, M. L., and Thoms, K. R., ADIP Quarterly Progr. Rep. June , 30, 1980, DOE/ER0045/3, p. 18.

[4] Braski, D. N., Carpenter, R. W., Bently, J., "The Microstructure of Ordered $(Co_{0.78}Fe_{0.11})_3V$ Alloy," ORNL/TM-7702, May 1981 and accepted for publication in Acta Metallurgica.

[5] Gittus, J., Irradiation Effects in Crystalline Solids, Applied Science Publ., Ltd., London (1978) p. 131.

[6] Braski, D. N. and Farrell, K. Electron Microscopy Vol. I, published by 7th European Congress on Electron Microscopy, (1980) p. 284.

[7] Stoloff, N. S. and Davies, R. G. Acta Met. 12 (1964) 473–485.

[8] Marankowski, M. J. Brown, N., and Fisher, R. M., Acta Met. 9 (1961) 137.

[9] Cottrell, A. H., p. 131 in Relation of Properties to Microstructure, ASM, Cleveland, Ohio (1954).

REFERENCES

[1] Liu, C. T., J. Nucl. Mater. 85&86 (1979) 907–911.

[2] Braski, D. N., The Resistance of $(Fe,Ni)_3V$ Long-Range Ordered Alloys to Neutron and Ion Irradiation, Proc. 2nd Topical Meeting - Fusion Reactor Materials, Seattle, Washington, 1981, to be published in Journal of Nuclear Materials.

[3] Grossbeck, M. L., and Thoms, K. R., ADIP Quarterly Progr. Rep. June , 30, 1980, DOE/ER0045/3, p. 18.

[4] Braski, D. N., Carpenter, R. W., Bently, J., "The Microstructure of Ordered $(Co_{0.78}Fe_{0.11})_3V$ Alloy," ORNL/TM-7702, May 1981 and accepted for publication in Acta Metallurgica.

[5] Gittus, J., Irradiation Effects in Crystalline Solids, Applied Science Publ., Ltd., London (1978) p. 131.

[6] Braski, D. N. and Farrell, K. Electron Microscopy Vol. I, published by 7th European Congress on Electron Microscopy, (1980) p. 284.

[7] Stoloff, N. S. and Davies, R. G. Acta Met. 12 (1964) 473–485.

[8] Marankowski, M. J. Brown, N., and Fisher, R. M., Acta Met. 9 (1961) 137.

[9] Cottrell, A. H., p. 131 in Relation of Properties to Microstructure, ASM, Cleveland, Ohio (1954).

[10] Biggs, W. D., and Broom, T., Phil. Mag. 45 (1954) 246.

[11] Davies, R. G., and Stoloff, N. S., Acta Met. 2 (1963) 1349.

[12] Marcinkowski, M. J. pp. 384 and 390 in Order-Disorder Transformations in Alloys, ed., Warlimont, H., Springer-Verlag, New York (1974).

[13] Braski, D. N., Schroeder, H., and Ullmaier, H., J. Nucl. Mater. 83 (1979) 265–277.

[14] Kangilaski, M., Perrin, J. S., and Wullaert, R. A., p. 83 in Irradiation Effects in Structural Alloys for Thermal and Fast Reactors, ASTM-STP-457 (1968).

[15] Bloom, E. E. and Weir, Jr., J. R., Nucl. Technol. 16 (1962) 45–54.